frontiers | Frontiers in Earth Science

TYPE Original Research
PUBLISHED 22 August 2022
DOI 10.3389/feart.2022.972642

OPEN ACCESS

EDITED BY
Mario Sprovieri,
National Research Council (CNR), Italy

REVIEWED BY
Zhixiong Shen,
Coastal Carolina University,
United States
Selvaraj Kandasamy,
Xiamen University, China

*CORRESPONDENCE
Xiaomei Nian,
xmnian@sklec.ecnu.edu.cn
Zhanghua Wang,
zhwang@geo.ecnu.edu.cn

SPECIALTY SECTION
This article was submitted to Marine Geoscience, a section of the journal Frontiers in Earth Science

RECEIVED 18 June 2022
ACCEPTED 18 July 2022
PUBLISHED 22 August 2022

CITATION
Niu W, Nian X, Zhao L, Zhai Y, Meadows ME, Zhang W and Wang Z (2022), Luminescence characteristics of muddy sediments in the turbidity maximum zone of the Yangtze River mouth and implications for the depositional mechanisms. *Front. Earth Sci.* 10:972642. doi: 10.3389/feart.2022.972642

Luminescence characteristics of muddy sediments in the turbidity maximum zone of the Yangtze River mouth and implications for the depositional mechanisms

Wenlei Niu[1,2], Xiaomei Nian[1]*, Luo Zhao[3], Yang Zhai[3], Michael E Meadows[4,5,6], Wentong Zhang[1] and Zhanghua Wang[1,2]*

[1]State Key Laboratory of Estuarine and Coastal Research, East China Normal University, Shanghai, China, [2]Southern Marine Science and Engineering Guangdong Laboratory (Zhuhai), Zhuhai, China, [3]Protection Center of Cultural Relics, Shanghai, China, [4]Department of Environmental & Geographical Science, University of Cape Town, Cape Town, South Africa, [5]School of Geography and Ocean Sciences, Nanjing University, Nanjing, China, [6]College of Geography and Environmental Sciences, Zhejiang Normal University, Jinhua, China

Muddy sediments are the most prominent constituents of sedimentary successions in tide-dominated river deltas and have highly complex depositional mechanisms. In this study, we performed fine-grained (4–11 μm) quartz optically stimulated luminescence (OSL) dating on two sediment cores collected at a shipwreck site in the turbidity maximum zone (TMZ) of the modern Yangtze River mouth, China, which were compared with previously published dating results including 45–63 um quartz OSL dating, radionuclide dating, porcelain artifacts recovered from the wreck, macro-plastics, and the morphological history recorded in marine charts. We investigate the luminescence characteristics of muddy sediments trapped in the TMZ and discuss the implications of OSL ages in understanding depositional mechanisms in tide-dominated river mouths. The results indicate that most OSL ages of muddy sediments in the delta front setting are overestimated compared with other dating methods. We suggest that OSL age overestimation reflects the trapping of sediments from offshore in the TMZ imported by saltwater intrusions and storm events. The offshore inputs contain high percentages of residual luminescence and are also subjected to incomplete bleaching due to turbid water conditions and near-bed dispersal in the salt-wedge river mouth. We thus suggest that the reduced bleaching efficiency of muddy sediments in delta front settings needs to be accounted for in understanding sedimentary processes and distinguishing between different sedimentary facies in tide-dominated river mouths. Furthermore, we propose that differences in quartz OSL ages of fine- and medium-grained fractions may arise in response to extreme events.

KEYWORDS

tide-dominated river mouth, OSL age overestimation, offshore inputs, residual luminescence, saltwater intrusion, storm event

Introduction

Muddy sediment is very prominent in sedimentary sequences of tide-dominated river deltas and is deposited in a range of sedimentary environments such as in channels and tidal flats (Dalrymple and Choi, 2007). However, it is difficult to distinguish between the sedimentary successions of tidal flats and distributary channels owing to the fact that both are characterized by interbedded sand and mud layers (Hori et al., 2001). Optically stimulated luminescence (OSL) dating (Aitken, 1998) may provide insights regarding the depositional mechanisms of such muddy sediments accumulated in channels of tide-influenced river mouths which are generally characterized by turbid water conditions, particularly in the turbidity maximum zone (TMZ) (Geyer, 1988; Burchard et al., 2018). As a consequence, incomplete surface and in-transport bleaching of muddy sediments may produce overestimated OSL ages in such circumstances. Moreover, storm events may introduce large volumes of fluid mud into the tide-dominated river mouth from offshore, with suspended sediment concentrations of between 10 and >100 g/L recorded near the sea bed (Ge et al., 2020). Such fluid mud may contain substantial quantities of reworked, older sediments with high percentages of residual luminescence. Thus, understanding the luminescence characteristics of muddy sediments in tide-influenced or tide-dominated deltaic successions is valuable in improving the interpretation of associated depositional mechanisms.

The Yangtze River Delta is a typical tide-dominated river delta (Figure 1; Goodbred and Saito, 2012) and there have

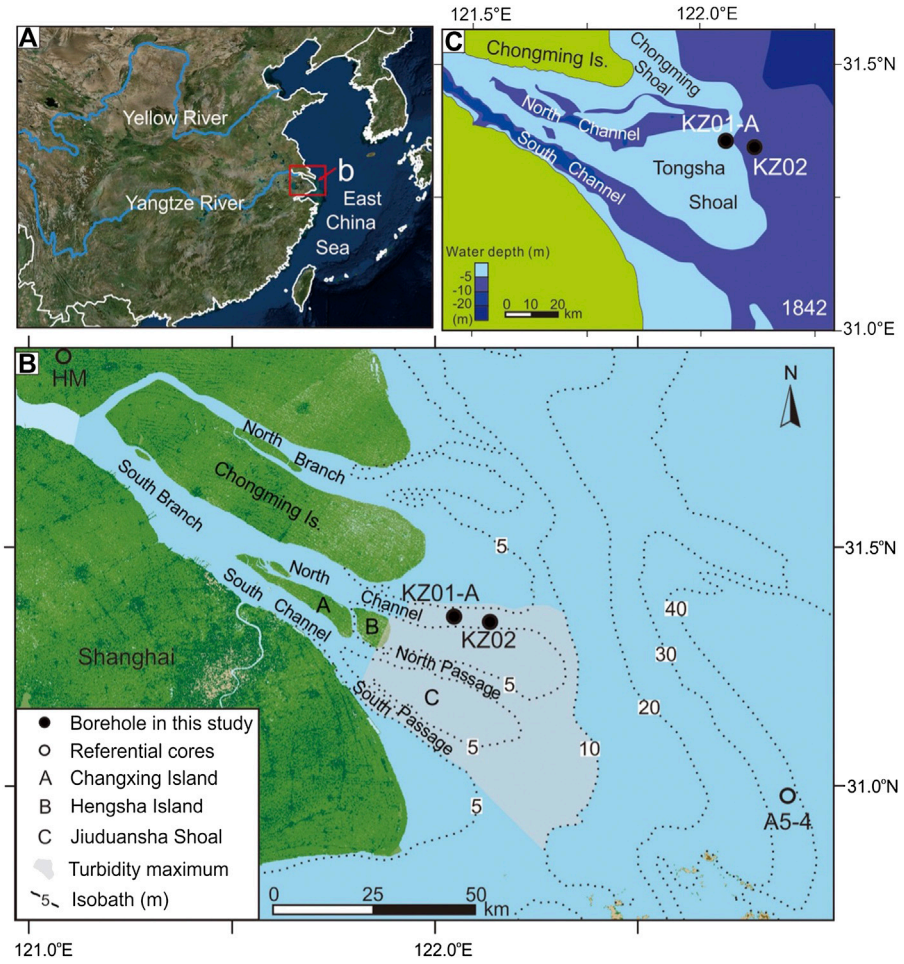

FIGURE 1
Location maps. **(A)** Yangtze River mouth (after Niu et al., 2021). **(B)** Locations of cores KZ01-A and KZ02 in the present-day North Channel and the turbidity maximum zone (TMZ; after Shen and Pan, 2001). **(C)** Bathymetry of the Yangtze River mouth in 1842 CE, showing the location of core KZ01-A at the northeast margin of the Tongsha Shoal and core KZ02 at water depth between 5 and 10 m (the delta front slope) (after Niu et al., 2021). The bathymetry map of 1842 CE is based on the marine chart of the British Navy. Core A5-4 was collected from Cheng et al. (2020). Core HM was collected from Nian et al. (2021).

been a number of studies using OSL to date its Holocene sediments (Sugisaki et al., 2015; Wang et al., 2015; Nian et al., 2018a, 2018b, 2019, 2021; Nian and Zhang, 2018; Wang et al., 2018, 2019). Wang et al. (2015) reported consistent OSL ages of fine-grained (4–11 μm) and coarse-grained (100–200 μm) quartz in a late Quaternary sediment core located in the pro-delta of the Yangtze River mouth. In contrast, in the palaeo-incised valley, Nian et al. (2018a, 2018b) reported incomplete bleaching of coarse-grained (90–125 μm or 150–180 μm) quartz in early to mid-Holocene sediments. Nian et al. (2021) further reported overestimated fine-silt quartz OSL ages of recent delta front sediments and attributed this to incomplete bleaching. Taking the Yangtze River mouth as an example, this paper aims to investigate the OSL dating results of different mud fractions of recent delta-front sediments in order to further elucidate our understanding of sedimentary mechanisms in tide-dominated river deltas.

In 2017, we collected two sediment cores (KZ01-A and KZ02) in the offshore section of the North Channel, which is located in the TMZ and the delta front platform of Yangtze River mouth (Figure 1; Niu et al., 2021). Core KZ01-A was collected at a shipwreck site; core KZ02 was collected in the Channel ca. 10 km seaward of the shipwreck site. Previously published AMS ^{14}C ages in the two cores suggested that the dated materials are mostly reworked from older deposits (Niu et al., 2021). Niu et al. (2021) also reported the overestimated medium-grained (45–63 μm) quartz ages compared with the age of porcelain artifacts recovered from the sunken ship. In this study, we further examined the fine-grained (4–11 μm) quartz OSL ages in these two cores and made comparison with results of other dating techniques, including the medium-grained OSL ages and ages inferred from ^{210}Pb and ^{137}Cs dating, porcelain artifacts, and macro-plastic distribution. We also used the evolutional history recorded in marine charts and literatures to constrain the chronologies of the two cores. We suggest that this study can broaden the application of OSL technique in the investigation of sedimentary processes in the fluvial-marine transitional environment, particularly in the tide-dominated or tide-influenced river mouths.

Geographical setting

The Yangtze River mouth, with a length of 120 km and a width of 90 km at its outer limit, is characterized by four outlets of three-tier bifurcations (Figure 1B; Chen et al., 1988). The main river is primarily divided by Chongming Island into the North Branch and South Branch, which is then separated into its North Channel and South Channel by Changxing-Hengsha Island (Figure 1B). The South Channel is further subdivided into North and South Passages by the Jiuduansha Shoal (Figure 1B). At present, more than 98% of the Yangtze River freshwater discharges through the South Branch into the sea, and the North Branch has become a tide-dominated abandoned channel (Dai et al., 2016). The North Channel is the largest distributary channel of the Yangtze River mouth, discharging around 50% of the freshwater and suspended sediments into the East China Sea (Mei et al., 2018).

The bifurcation pattern described above formed less than 200 years ago (Figure 2; Chen et al., 1988; Li et al., 2011). According to the earliest marine charts of the Yangtze River mouth, the Changxing-Hengsha Island had not separately emerged by the mid-19th century and was connected to the Tongsha Shoal at the river mouth (Figures 1C). The South Channel had formed by that time and was the major distributary channel discharging most of the freshwater and suspended sediments from the South Branch (Chen et al., 1988). A flood-dominated channel was present at the site of North Channel, which was closed at the upstream end by sand shoals connected to the Chongming Island, and with water depth <5 m at its downstream end (Figure 1C). In the late 19th century, the upstream end of the flood-dominated North Channel was forced open by extreme Yangtze River floods (Figure 2A) and then became an important pathway for freshwater and suspended sediment discharge (Chen et al., 1988; Li et al., 2011; Mao, 2014). At the beginning of the 20th century, water depth at the downstream end of the North Channel increased, possibly flushed by the Yangtze floods (Figure 2B; Mei et al., 2018). The northern margin of the Tongsha Shoal was subject to ongoing erosion in the 20th century (Chen et al., 1988), which exposed the previously buried shipwreck site in the North Channel (Figure 2C). In addition, in the mid-20th century, the formation of the North Passage made the Jiuduansha Shoal independent from the Tongsha Shoal (Figure 2C), and the present pattern of the four outlets at the Yangtze River mouth was then established (Figure 2D; Chen et al., 1988; Li et al., 2011; Mao, 2014; Su and Fan, 2018).

Tidal range at the Yangtze River mouth is between 2 and 4 m, with a mean value of 2.66 m (Chen et al., 1988), but may reach 5 m during summer and autumn typhoon events. The average wave height is 0.9 m in fair weather, while maximum wave height exceeds 6 m during stormy conditions (Zhu et al., 1988). The wave base is ca. -10 m in the fair weather and reaches -30 m in storms (Xu et al., 1989). The TMZ occurs at the delta front platform where the mouth shoals and subaqueous distributary channels dominate; suspended sediment concentration (SSC) is 0.1–0.7 g/L near the water surface but is much greater (1–8 g/L) near the bed (Shen et al., 1992; Li and Zhang, 1998; Shen and Pan, 2001). Fluid mud is always observed at slack tides in the tide-dominated channels, particularly at the head of the salt wedge and in storm conditions, reaching a biggest thickness of ca. 0.9 m (Shen and Li, 2011; Ge et al., 2018, 2020).

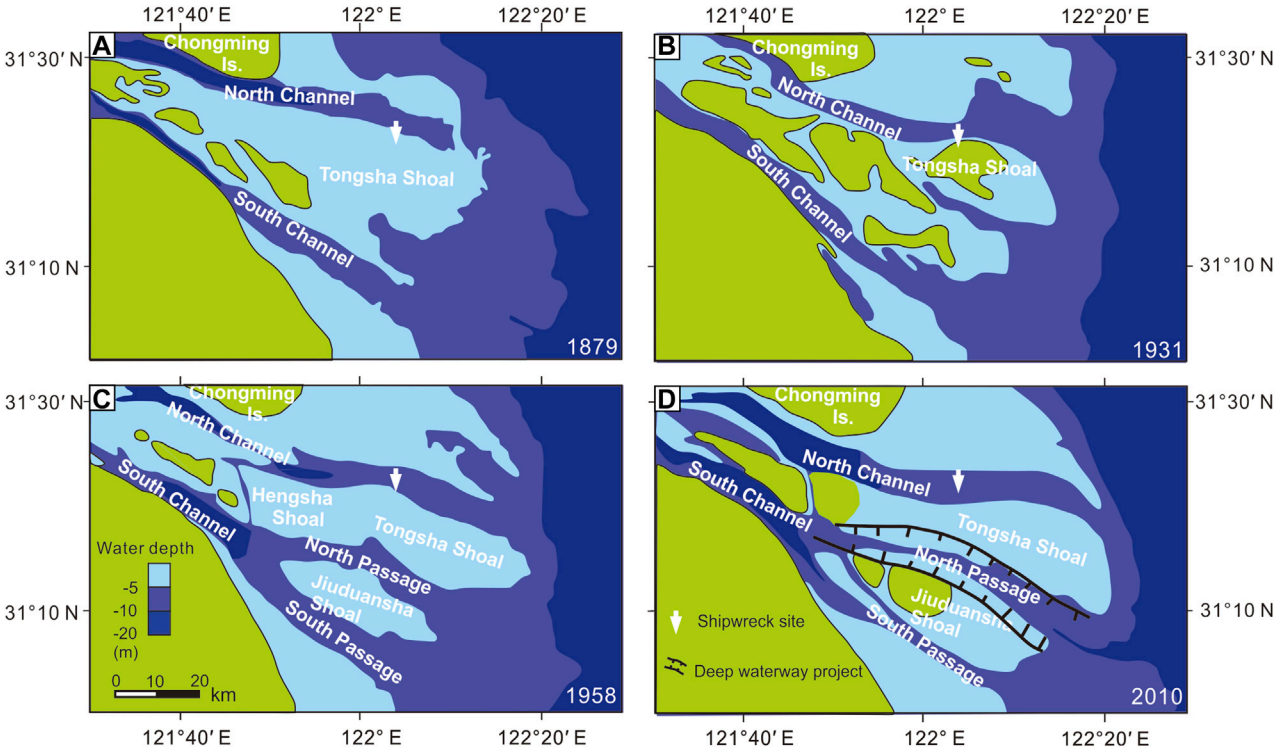

FIGURE 2
Historical marine charts showing morphological changes of the Yangtze River mouth from 1879 to 2010 CE (after Su and Fan, 2018).

Materials and methods

Lithostratigraphy and sedimentary facies of two sediment cores

Cores KZ01-A (31°21′02.962″ N, 122°04′E) and KZ02 (31°19′50.610″ N, 122°10′E) were obtained using rotary drilling in October 2017 in the subaqueous section of the North Channel, Yangtze River mouth (Figure 1), to study the sedimentary environmental evolution at the shipwreck site (Niu et al., 2021). Water depth at the two core sites was measured at 9.0 and 7.8 m below mean sea level (Yellow Sea datum of 1985), respectively. Core KZ01-A is 13.8 m long and core KZ02 is 13.9 m long; core diameter is 10 cm in both cores.

Six depositional units are identified in the stratigraphy of core KZ01-A from the base upwards (Figure 3A; Niu et al., 2021): homogeneous prodelta mud (unit I, 13.8–8.25 m), interbedded sand and mud of delta front slope (unit II, 8.25–7.4 m), mouth shoal sand (unit III, 7.4–6.78 m), flood-dominated channel mud (unit IV, 6.78–4.15 m), storm deposits containing the woods of sunken ship (unit V, 4.15–3.22 m), mouth shoal sand and interbedded sand and mud of subaqueous distributary channel (unit VI-1, 3.22–2.45 m; unit VI-2, 2.45–0 m). Macro-plastics are evident at depths 2.84–2.89 and 1.5 m (unit VI). Core KZ02 is divided into four depositional units in ascending order as follows (Figure 3B): prodelta mud (unit I, 13.9–8.6 m), interbedded sand and mud of delta front slope (unit II, 8.60–7.75 m), mouth shoal sand (unit III, 7.75–2.58 m) and interbedded sand and mud of subaqueous distributary channel (unit IV, 2.58–0 m).

The sunken ship at the site of core KZ01 contains porcelain artifacts of the late Qing dynasty (Niu et al., 2021). Some porcelain artifacts have been engraved on the bottom with characters “同治” (Tongzhi, the title of an emperor during 1862–1875 CE), which provides a maximum age for the shipwreck (and therefore unit V of core KZ01-A) of 1862 CE (Niu et al., 2021). Based on China’s plastics production report (CPCIA, 1984–2014), the macro-plastics found in unit VI of core KZ01-A constrain the age of this unit to post-1950 CE.

Sample preparation and measurements for OSL dating

Six samples in core KZ01-A and four samples in core KZ02 were carefully collected for OSL dating, and ages of their medium-grained fractions are reported in Niu et al. (2021) (Figure 3). For this study, we applied OSL dating to

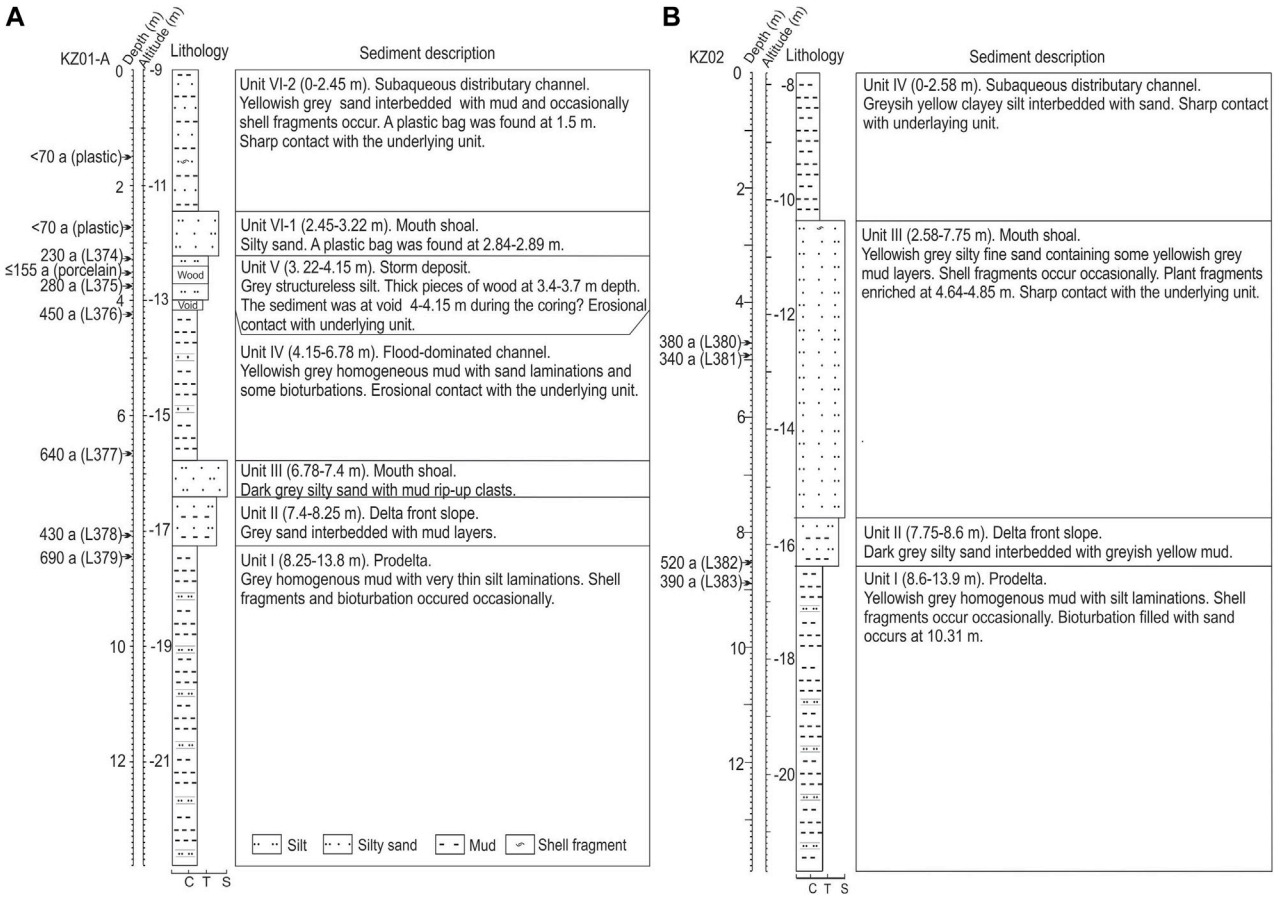

FIGURE 3
Lithostratigraphy and interpretation of sedimentary facies in cores KZ01-A **(A)** and KZ02 **(B)** (after Niu et al., 2021). Laboratory numbers of OSL samples, MAM ages of medium-grained quartz, age of porcelain artifacts discovered in the sunken ship, and ages of macro-plastics are indicated on the left side of the profiles (after Niu et al., 2021). All ages are calibrated to before 2017 CE.

the fine-grained (4–11 μm) quartz fraction. The samples were firstly treated with HCl and H_2O_2 to remove carbonates and organic matter, respectively. After collecting the fine-grained fractions based on Stokes' law, these were etched with 30% H_2SiF_6 for three to four days, followed by washing with HCl and distilled water to extract pure quartz grains. The fine-grained fraction was settled in acetone and deposited on stainless steel discs. The purity of quartz was examined by detecting the infrared-stimulated luminescence following the method of Duller (2003).

All OSL measurements were carried out using a Risø TL/OSL DA-20 DASH reader with 7.5 mm Hoya U-340 filters in front of an ET EMD-9107 photomultiplier tube. Laboratory irradiation was produced by a calibrated beta $^{90}Sr/^{90}Y$ source. Blue LED stimulation (470 nm, 90% of 97 mW/cm^2 full power) and IR LED (870 nm, 90% of 129 mW/cm^2 full power) were used in the measurement. The equivalent dose (D_e) of the quartz grains was determined by the single-aliquot regenerative-dose (SAR) protocol (Murray and Wintle, 2003). A 200°C preheat for 10 s and a 160°C cut-heat for 0 s were used in the SAR protocol, and all luminescence measurements were made by blue stimulation at 125°C for 40 s; the experimental conditions were chosen based on the results of medium-grained quartz (Niu et al., 2021; Supplementary Figure S1). The late background method, i.e. the initial 0.4 s of stimulation subtracts a background signal derived from the last 10 s of stimulation, was used to estimate the D_e values using a single saturating exponential function.

Uranium (U), thorium (Th), and potassium (K) concentrations of OSL samples were estimated using neutron activation analysis (NAA) at the China Institute of Atomic Energy (Supplementary Table S1; Niu et al., 2021). The water content (weight of water/weight of dry sediments) was measured by weighing the samples before and after drying to constant weight (Table 1). Total dose rates were calculated using the software Dose Rate and Age Calculator ('DRAC') (Durcan et al., 2015). Concentrations of U, Th, and K were converted into dose rates using the conversion factors of Adamiec and Aitken (1998). An alpha efficiency factor (α-value) of 0.04 ± 0.02 (Rees-Jones, 1995) was used for fine-grained samples. Alpha-

TABLE 1 Summary of fine-grained (4–11 μm) quartz OSL dating results in this study and pervious published OSL data of medium-grained (45–63 μm) quartz (Niu et al., 2021) in cores KZ01-A and KZ02. OSL ages are relative to 2017 CE.

Borehole	Lab No.	Depth (m)	Lithology	Unit	Sedimentary facies	Water content (%)	Grain size (μm)	Dose rate (Gy/ka)	No. of aliquots	CAM-D_e (Gy)	CAM-Age (a)	[a]MAM-D_e (Gy)	MAM-Age (a)
KZ01-A	L374	3.20–3.37	Structureless silt	V	Storm deposit	35 ± 10	4–11	2.40 ± 0.17	6	0.68 ± 0.02	280 ± 20	–	–
							45–63	2.18 ± 0.14	20	0.73 ± 0.06	330 ± 30	0.51 ± 0.05	230 ± 20
	L375	3.69–3.82	Structureless silt	V	Storm deposit	20 ± 10	4–11	2.93 ± 0.23	6	0.83 ± 0.02	280 ± 20	–	–
							45–63	2.65 ± 0.18	20	0.92 ± 0.06	340 ± 20	0.75 ± 0.07	280 ± 20
	L376	4.15–4.30	Homogeneous mud	IV	Flood-dominated	44 ± 10	4–11	2.98 ± 0.20	6	1.33 ± 0.03	450 ± 30	–	–
					channel		45–63	2.70 ± 0.16	25	1.71 ± 0.15	630 ± 60	1.22 ± 0.12	450 ± 50
	L377	6.56–6.63	Homogeneous mud	IV	Flood-dominated	28 ± 10	4–11	2.39 ± 0.17	6	1.45 ± 0.05	610 ± 50	–	–
					channel		45–63	2.21 ± 0.15	27	1.55 ± 0.07	700 ± 40	1.43 ± 0.06	640 ± 30
	L378	8.03–8.13	Sand interbedded with mud	II	Delta front slope	41 ± 10	4–11	3.10 ± 0.22	6	1.48 ± 0.03	480 ± 40	–	–
							45–63	2.79 ± 0.16	26	1.47 ± 0.11	520 ± 40	1.21 ± 0.11	430 ± 40
	L379	8.40–8.50	Homogeneous mud	I	Prodelta	49 ± 10	4–11	2.98 ± 0.20	6	1.86 ± 0.04	620 ± 40	–	–
							45–63	2.71 ± 0.16	32	2.02 ± 0.09	740 ± 50	1.88 ± 0.06	690 ± 40
KZ02	L380	4.68–4.78	Silty fine sand	IV	Mouth shoal	63 ± 10	4–11	2.01 ± 0.13	6	2.02 ± 0.07	1,000 ± 70	–	–
							45–63	1.83 ± 0.10	19	0.82 ± 0.06	450 ± 40	0.71 ± 0.04	380 ± 30
	L381	4.88–4.98	Silty fine sand	IV	Mouth shoal	29 ± 10	4–11	2.68 ± 0.20	5	2.41 ± 0.14	900 ± 90	–	–
							45–63	2.41 ± 0.16	23	0.97 ± 0.05	400 ± 20	0.84 ± 0.07	340 ± 30
	L382	8.46–8.54	Sand interbedded with mud	II	Delta front slope	29 ± 10	4–11	2.48 ± 0.19	3	2.03 ± 0.12	820 ± 80	–	–
							45–63	2.23 ± 0.15	24	1.27 ± 0.08	560 ± 40	1.17 ± 0.04	520 ± 20
	L383	8.81–8.89	Homogeneous mud	I	Prodelta	44 ± 10	4–11	3.40 ± 0.23	6	1.29 ± 0.03	380 ± 30	–	–
							45–63	3.08 ± 0.19	24	1.40 ± 0.06	450 ± 30	1.22 ± 0.09	390 ± 30

[a]The 45–63 μm OSL dating studies are carried out using small aliquots of quartz (2 mm mask size). The sigma-b value of 0.1 was used for the minimum age model (MAM) calculations of 45–63 μm quartz according to the previous studies in the area (Nian et al., 2018a; 2018b).

10.3389/feart.2022.972642

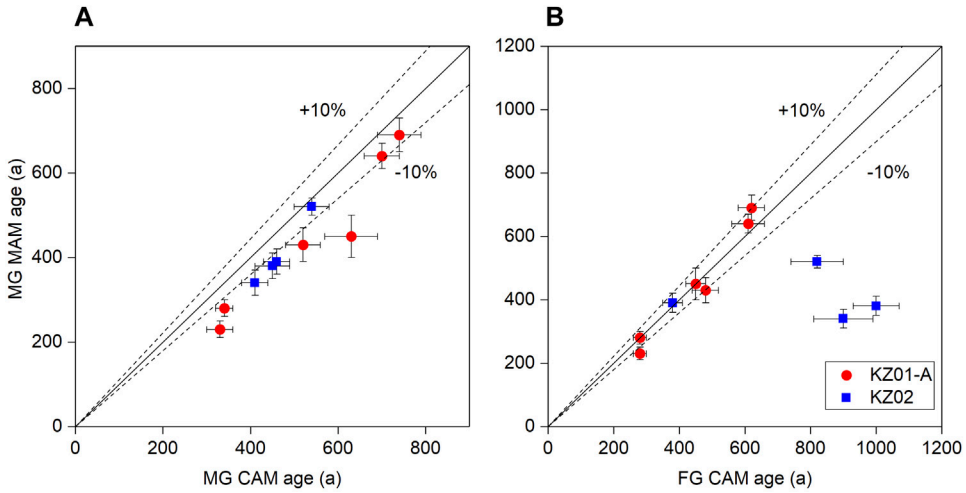

FIGURE 4
Comparisons of the CAM and MAM ages of medium-grained quartz samples **(A)**; and CAM ages of fine-grained samples and MAM ages of medium-grained samples **(B)** in cores KZ01-A and KZ02. The OSL data of medium-grained samples are from Niu et al. (2021).

attenuation factors of Brennan et al. (1991) and beta-attenuation factors of Guérin et al. (2012) were used to calculate the dose rates, respectively. OSL ages are relative to 2017 CE.

Results

Fine-grained quartz OSL ages

The OSL decay and dose-response curve for the representative fine-grained quartz sample L379 are shown in Supplementary Figure S2. Rapid decay of the signals with stimulation time indicates that the signals of quartz in the sediments are dominated by the fast component (Supplementary Figure S2A), which is consistent with previous studies in the area (Nian and Zhang, 2018; Nian et al., 2019). A single exponential function of the growth curve was constructed using five regenerative dose points including a zero-dose measurement and a recycling point (Supplementary Figure S2B). The central age model (CAM) (Galbraith et al., 1999) was applied for D_e calculation, which yielded OSL ages of 280–620 a and 380–1,000 a in cores KZ01-A and KZ02, respectively, (Table 1).

Comparison of OSL ages between different grain-size fractions

The CAM ages of medium-grained quartz (330–740 a in core KZ01-A; 400–560 a in core KZ02) are approximately 40–180 a older than the corresponding ages calculated by minimum age model (MAM) (230–690 a in core KZ01-A; 340–520 a in core KZ02) in these two cores (Table 1; Figure 4A; Niu et al., 2021). Supplementary Figure S3 presents radial plots of medium-grained D_e values of these ten samples, showing that some samples exhibit an asymmetric tail of higher D_e values and display varying degrees of D_e scatter. Thus, medium-grained MAM ages should provide more reliable depositional time and were used for the age comparisons below.

In core KZ01-A, the CAM ages of fine-grained samples are generally consistent with medium-grained MAM ages within each error condition (Table 1; Figure 4B), and the paired OSL ages obtained from two different grain-size fractions generally increase with stratigraphic depth as expected, with the exception of sample L377 which exhibits age reversal (Figure 5A). Such OSL age reversals have been reported previously in the Yangtze Delta (Nian and Zhang, 2018; Wang et al., 2019). In core KZ02, significant reversals of fine-grained quartz OSL ages were observed, ranging from ca. 380 a to 1,000 a from the bottom upward, and the ages are ca. 300–600 a older than the corresponding medium-grained quartz MAM ages, except for sample L383 from prodelta unit which has consistent paired ages (Table 1; Figures 4B and Figure 5B).

Comparison of OSL ages with other dating results

The evolutional history of the North Channel is recorded in marine charts (Chen et al., 1988; Li et al., 2011; Mao, 2014; Mei et al., 2018), which can therefore help to constrain the OSL and

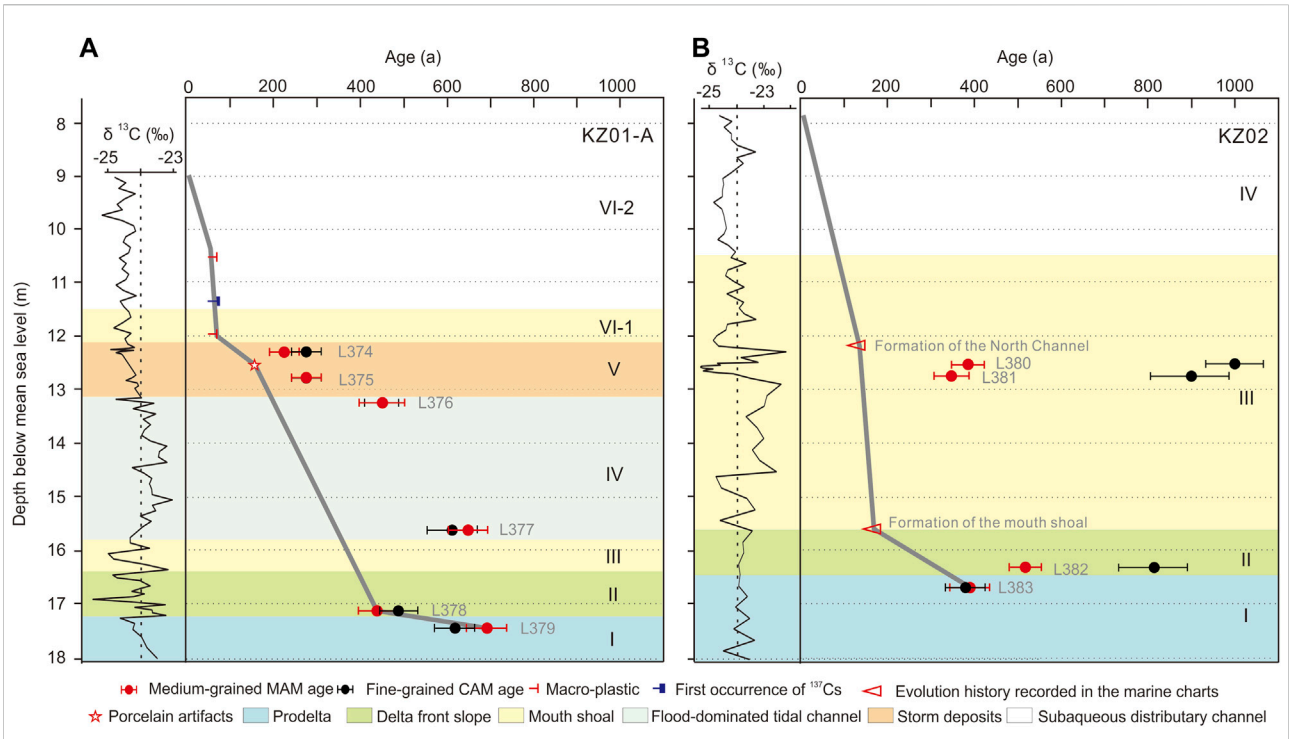

FIGURE 5
Comparison of various chronologies obtained in cores KZ01-A **(A)** and KZ02 **(B)**. Core depths are calibrated into depths below the mean sea level. The $\delta^{13}C$ curves and evolution history of North Channel are from Niu et al. (2021). Unit numbers are as in Figure 3. The solid line indicates the best estimated age-depth curve.

radionuclide chronologies. It can be observed in the marine chart of 1842 CE (175 a; Figure 1C) that the two core localities were at that time situated in the mouth shoal (i.e., the Tongsha Shoal) and at the edge of the mouth shoal, respectively. This suggests that the delta front slope environment at sites of both cores would have been formed before 175 a, and the mouth shoal environment at core site KZ02 would have been formed after 175 a. Moreover, previous studies have reported that the North Channel only evolved from the flood-dominated channel to become the major distributary channel at the end of 19th century (≤117 a; Figure 2; Chen et al., 1988; Li et al., 2011; Mao, 2014). This reconstructed evolution is supported by the observation that $\delta^{13}C$ values in the upper sections of two cores are consistently more depleted, because increased freshwater discharge would have supplied more terrestrial-sourced organic carbon to the core sites (Figure 5; Niu et al., 2021). Thus, the mouth shoal sands with less depleted $\delta^{13}C$ values in the lower section of core KZ02 would have been deposited between 175 a and 117 a, which suggests that OSL ages of L380 (380 ± 30 a) and L381 (340 ± 30 a) are overestimated by ca. 200–250 a (Figure 5B).

Furthermore, in core KZ01-A, the age of unit V containing the shipwreck wood is constrained by the porcelain artifacts which indicate an age younger than 1862 CE (≤155 a; Figure 5A; Niu et al., 2021); the macro-plastic deposits (Figure 3A), together with the ^{210}Pb and ^{137}Cs results (Supplementary Figure S4), clearly point to a younger age for unit VI (CPCIA, 1984–2014; Niu et al., 2021). Thus, unit V in KZ01-A would have been deposited post-1862 CE but before 1950 CE, indicating that the determined OSL ages are overestimated by ca. 100 a. Previous studies reported a residual OSL age of ca. 60 a in modern fine-grained quartz from the Yangtze riverine inputs (Sugisaki et al., 2015; Wang et al., 2018). However, above OSL ages are still overestimated after deducting 60 a.

Discussion

Reasons for overestimation of OSL ages

Comparison between multiple dating methods indicates that OSL ages of delta front sediments in Yangtze River mouth are in general overestimated. We suggest that the OSL age overestimation is a characteristic of muddy sediments trapped in the TMZ of tide-dominated river deltas because sunlight transmission in the water column is substantially reduced by the turbidity of the water. Ditlefsen (1992) recorded experimentally that light levels at 75-cm depth

in a water column with 0.05 g/L suspended sediment concentration was <0.01% of that measured at the water surface. Meanwhile, Richardson (2001) reported that light levels were reduced by three orders of magnitude in the upper 80 cm of a turbid water column in the near-coast environment of England. The experiment by Sanderson et al. (2007) in the Mekong Delta revealed a similar substantial reduction of light levels in water with moderate turbidity. Given that suspended sediment concentrations near the water surface in the TMZ of Yangtze River mouth reach 0.1–0.7 g/L (Shen et al., 1992; Li and Zhang, 1998; Shen and Pan, 2001), sunlight intensity would be markedly reduced in the water column, thus constraining quartz bleaching of in-transport sediments.

Secondly, we suggest that the sediments from offshore trapped in the saltwater wedge make a major contribution to the overestimated OSL ages. The less depleted $\delta^{13}C$ values observed in both cores KZ01-A and KZ02 are indicative of a major contribution from marine-sourced organic carbon in the delta front setting (Figure 5; Niu et al., 2021). The offshore inputs into the Yangtze River mouth have been reported in many previous studies (e.g., Du et al., 2010; Ge et al., 2020; Wang et al., 2021) and surficial sediments in the subaqueous delta have yielded OSL ages exceeding 1,000 a (e.g., core A5-4 in Cheng et al., 2020; see Figure 1B for the core location). When older sediments are imported into the river mouth by processes such as tidal pumping, estuarine circulation induced by saltwater intrusion, and storm events (Warner et al., 2008; Cho et al., 2012; Li et al., 2016; Burchard et al., 2018; Wang et al., 2020), they are less likely to be bleached because the stratified water column suppresses turbulence and the sediments have no chance to be dispersed to the water surface. Moreover, thick benthic layer of fluid mud in the channel of Yangtze River mouth have been observed in the typhoon condition; numerical experiments indicate that the typhoon wind strongly enhances saltwater intrusion and therefore intensifies the degree of water stratification, leading to the formation and near-bed movement of the fluid mud layer from offshore region into the channel (Ge et al., 2018; 2020). Such fluid mud is more likely to be preserved in the sedimentary sequence because it is not completely resuspended by currents in subsequent fair weather (Dalrymple and Choi, 2007).

In tide-dominated river deltas, turbid water conditions, reworked offshore sediments, and complex sediment transport and deposition processes related to saltwater intrusion and storm events may, therefore, all contribute to overestimation of substantial OSL ages. However, owing to spatial variation in OSL ages of offshore surficial sediments (Sugisaki et al., 2015; Wang et al., 2018; Cheng et al., 2020), coupled with the dynamic nature of evolution in the subaqueous delta, it is difficult to estimate the degree of overestimation. For example, Nian et al. (2021) reported OSL age overestimation of between ca. 500–2000 a for delta front sediments in core HM obtained from the modern Yangtze delta plain (core location shown in Figure 1B), which is substantially greater than values reported herein. This suggests that further research involving a systematic investigation of residual luminescence of suspended and surficial sediments in the river mouth is necessary to resolve such differences.

Implications of overestimated OSL ages for depositional mechanisms

Based on the above discussion, we propose that bleaching efficiency of the fine and medium-sized quartz grains may be useful in identifying the depositional mechanisms in the tide-dominated river delta. For example, the overestimated OSL ages can be used to differentiate between sedimentary sequences at the delta front from those of tidal flats, which otherwise have similar sedimentary structures. Accordingly, exposure during ebb tides and resuspension in the shallow waters of the intertidal and subtidal zone favours stronger bleaching (Madsen et al., 2007; Mauz et al., 2010). Moreover, since incomplete bleaching is related to water column stratification as outlined above, OSL age differences can also be used to distinguish the salt-wedge river mouth settings from those slightly stratified or vertically mixed ones. In contrast, in slightly stratified or vertically mixed river mouths where turbulence prevails, the suspended sediments are much more effectively bleached.

Comparison of OSL ages obtained from different grain-size fractions may further indicate the depositional mechanisms of muddy sediments in a delta front setting. We consider that OSL age consistency between fine- and medium-grained samples collected from the flood-dominated channel facies (unit IV in core KZ01-A; Table 1; Figures 4B and Figure 5A) indicates that the two fractions are products of the same source and depositional processes. Taken together with observations of age overestimation, it is proposed that muddy sediments are mainly deposited by processes associated with saltwater intrusions, which introduce offshore inputs via near-bed movement of the dense current (Geyer, 1993; Burchard et al., 2018; Ge et al., 2018). This interpretation is supported by the observation that $\delta^{13}C$ values here are markedly less depleted (Figure 5A), which indicates a major contribution of marine-sourced organic carbon. Furthermore, it concurs with our conclusion that this unit represents sediments formed in a flood-dominated channel (Niu et al., 2021), where the freshwater discharge is constrained in the surface and trapping of sediments is mainly associated with tide pumping and estuarine circulation.

In contrast, OSL ages of fine-grained fractions are significantly older than those of the medium-grained fractions

in mouth shoal sediments of KZ02 (Figure 5B), suggesting that the two fractions have different depositional processes. The mouth shoal sediments are comprised of sediments that are better sorted and are more completely bleached because they are frequently resuspended by waves in fair weather. We therefore argue that rapid deposition of sediments reworked in extreme events may produce inconsistent OSL ages for the different size fractions, which is further evidenced by the strong fluctuations in $\delta^{13}C$ values of the mouth shoal sediments (Figure 5B).

Conclusion

Two sediment cores KZ01-A and KZ02 were collected in the subaqueous distributary channel (the North Channel) of the Yangtze River mouth in 2017. We conducted quartz OSL dating on the fine-grained fractions (4–11 μm) in this study. Together with previously published ages from medium-grained quartz fractions (45–63 μm), radionuclide dating, porcelain artifacts recovered from a sunken ship, macro-plastics, and the evolutionary history of the North Channel recorded in marine charts, the study reveals that understanding the ages of muddy sediments casts light on the complexity of depositional processes in the tide-dominated river delta. The following conclusions are drawn:

1. OSL ages obtained from muddy sediments in the delta front setting of the Yangtze River mouth are in general overestimated, which we infer results from high turbidity of the water, reworked, older offshore sediments, and the sediment dispersal and trapping processes related to saltwater intrusion and storm events in the TMZ.
2. The lower bleaching efficiency of muddy sediments trapped in the TMZ offers a useful proxy to distinguish delta front deposits in the highly stratified tide-influenced or tide-dominated river mouth, i.e., the salt-wedge type from those slightly stratified or well-mixed ones.
3. OSL ages of fine- and medium-grained fractions are more consistent in sediments deposited in the flood-dominated channel compared to those in the mouth shoal, which we interpret as indicating rapid deposition of reworked sediments by extreme storm events in the mouth shoal.

Data availability statement

The original contributions presented in the study are included in the article/Supplementary Material, further inquiries can be directed to the corresponding authors.

Author contributions

WN and WZ performed the laboratory analyses and data process. LZ and YZ drill the core and provided the archaeological finding. XN examined the OSL dating results. ZW designed the research. WN, ZW, and MM wrote the manuscript. All authors revised the manuscript.

Funding

This study was supported by Innovation Program of Shanghai Municipal Education Commission (2019-01-07-00-05-E00027) and Protection Center of Cultural Relics, Shanghai, China. WN was funded by the China Scholar Council Scholarship (CSC, 201806140087).

Acknowledgments

We thank Adam Switzer, Stephen Chua and Pavel Adamek for their help with revision of the manuscript. The authors are also grateful to Fengyue Qiu for his help with OSL age calculation.

Conflict of interest

The authors declare that the research was conducted in the absence of any commercial or financial relationships that could be construed as a potential conflict of interest.

Publisher's note

Supplementary Material

The Supplementary Material for this article can be found online at: https://www.frontiersin.org/articles/10.3389/feart.2022.972642/full#supplementary-material

References

Adamiec, G., and Aitken, M. J. (1998). Dose-rate conversion factors: update. *Anc. TL* 16 (2), 37–50.

Aitken, M. J. (1998). *An Introduction to Optical Dating*. New York: Oxford University Press.

Brennan, B. J., Lyons, R. G., and Phillips, S. W. (1991). Attenuation of alpha particle track dose for spherical grains. *Int. J. Radiat. Appl. Instrum. Part D. Nucl. Tracks Radiat. Meas.* 18, 249–253. doi:10.1016/1359-0189(91)90119-3

Burchard, H., Schuttelaars, H. M., and Ralston, D. K. (2018). Sediment trapping in estuaries. *Annu. Rev. Mar. Sci.* 10, 371–395. doi:10.1146/annurev-marine-010816-060535

Chen, J. Y., Shen, H. T., and Yun, C. X. (1988). *Processes of dynamics and geomorphology of the changjiang estuary*. Shanghai: Shanghai Science and Technical Publication. (In Chinese).

Cheng, Q. Z., Wang, F., Chen, J., Ge, C., Chen, Y. L., Zhao, X. Q., et al. (2020). Combined chronological and mineral magnetic approaches to reveal age variations and stratigraphic heterogeneity in the Yangtze River subaqueous delta. *Geomorphology* 359, 107163. doi:10.1016/j.geomorph.2020.107163

Cho, K. H., Wang, H. V., Shen, J., Valle-Levinson, A., and Teng, Y. C. (2012). A modeling study on the response of Chesapeake Bay to hurricane events of Floyd and Isabel. *Ocean. Model.* 49–50, 22–46. doi:10.1016/j.ocemod.2012.02.005

CPCIA (1984–2014). *China chemical industry yearbook*. Beijing: China Chemical Industry Publishing House. (in Chinese).

Dai, Z. J., Fagherazzi, S., Mei, X. F., and Gao, J. J. (2016). Decline in suspended sediment concentration delivered by the Changjiang (Yangtze) river into the east China sea between 1956 and 2013. *Geomorphology* 268, 123–132. doi:10.1016/j.geomorph.2016.06.009

Dalrymple, R. W., and Choi, K. (2007). Morphologic and facies trends through the fluvial-marine transition in tide-dominated depositional systems: A schematic framework for environmental and sequence-stratigraphic interpretation. *Earth. Sci. Rev.* 81 (3–4), 135–174. doi:10.1016/j.earscirev.2006.10.002

Ditlefsen, C. (1992). Bleaching of K-feldspars in turbid water suspensions: a comparison of photo and thermoluminescence signals. *Quat. Sci. Rev.* 11, 33–38. doi:10.1016/0277-3791(92)90039-b

Du, J. Z., Wu, Y. F., Huang, D. K., and Zhang, J. (2010). Use of ^{7}Be, ^{210}Pb and ^{137}Cs tracers to the transport of surface sediments of the Changjiang Estuary, China. *J. Mar. Syst.* 82 (4), 286–294. doi:10.1016/j.jmarsys.2010.06.003

Duller, G. A. T. (2003). Distinguishing quartz and feldspar in single grain luminescence measurements. *Radiat. Meas.* 37, 161–165. doi:10.1016/s1350-4487(02)00170-1

Durcan, J. A., King, G. E., and Duller, G. A. T. (2015). DRAC: Dose Rate and age calculator for trapped charge dating. *Quat. Geochronol.* 28, 54–61. doi:10.1016/j.quageo.2015.03.012

Galbraith, R. F., Roberts, R. G., Laslett, G. M., Yoshida, H., and Olley, J. M. (1999). Optical dating of single and multiple grains of quartz from jinmium rock shelter, northern Australia: Part 1, experimental details and statistical models. *Archaeometry* 41, 339–364. doi:10.1111/j.1475-4754.1999.tb00987.x

Ge, J. Z., Chen, C. S., Wang, Z. B., Ke, K. T., Yi, J. X., and Ding, P. X. (2020). Dynamic response of the fluid mud to a tropical storm. *JGR. Oceans* 125 (3), e2019JC015419. doi:10.1029/2019jc015419

Ge, J. Z., Zhou, Z. Y., Yang, W. L., Ding, P. X., Chen, C. S., Wang, Z. B., et al. (2018). Formation of concentrated benthic suspension in a time-dependent salt wedge estuary. *J. Geophys. Res. Oceans* 123, 8581–8607. doi:10.1029/2018jc013876

Geyer, R. (1993). The importance of suppression of turbulence by stratification on the estuarine turbidity maximum. *Estuaries* 16, 113–125. doi:10.2307/1352769

Geyer, W. R. (1988). "The advance of a salt wedge front: Observations and dynamical model," in *Physical processes in estuaries*. Editors J. Dronkers and W. van Leussen (Springer-Verlag), 181–195.

Goodbred, S. L., and Saito, Y. (2012). "Tide-dominated deltas," in *Principles of tidal sedimentology* (Dordrecht: Springer), 129–149.

Guérin, G., Mercier, N., Nathan, R., Adamiec, G., and Lefrais, Y. (2012). On the use of the infinite matrix assumption and associated concepts: A critical review. *Radiat. Meas.* 47, 778–785. doi:10.1016/j.radmeas.2012.04.004

Hori, K., Saito, Y., Zhao, Q., Cheng, X., Wang, P., Sato, Y., et al. (2001). Sedimentary facies of the tide-dominated paleo-Changjiang (Yangtze) estuary during the last transgression. *Mar. Geol.* 177, 331–351. doi:10.1016/s0025-3227(01)00165-7

Li, J. F., and Zhang, C. (1998). Sediment resuspension and implications for turbidity maximum in the Changjiang Estuary. *Mar. Geol.* 148, 117–124. doi:10.1016/s0025-3227(98)00003-6

Li, M. T., Chen, Z. Y., Yin, D. W., Chen, J., Wang, Z. H., and Sun, Q. L. (2011). Morphodynamic characteristics of the dextral diversion of the Yangtze River mouth, China: Tidal and the coriolis force controls. *Earth Surf. Process. Landf.* 36, 641–650. doi:10.1002/esp.2082

Li, X. Y., Zhu, J. R., Yuan, R., Qiu, C., and Wu, H. (2016). Sediment trapping in the changjiang estuary: Observations in the north passage over a spring-neap tidal cycle. *Estuar. Coast. Shelf Sci.* 177, 8–19. doi:10.1016/j.ecss.2016.05.004

Madsen, A. T., Murray, A. S., Andersen, T. J., and Pejrup, M. (2007). Optical dating of young tidal sediments in the Danish Wadden Sea. *Quat. Geochronol.* 2, 89–94. doi:10.1016/j.quageo.2006.05.008

Mao, Z. C. (2014). *Shanghai tidal flat research*. Shanghai: East China Normal University Press, 1–150. (In Chinese).

Mauz, B., Baeteman, C., Bungenstock, F., and Plater, A. J. (2010). Optical dating of tidal sediments: Potentials and limits inferred from the north sea coast. *Quat. Geochronol.* 5 (6), 667–678. doi:10.1016/j.quageo.2010.05.004

Mei, X. F., Dai, Z. J., Wei, W., Li, W. H., Wang, J., and Sheng, H. (2018). Secular bathymetric variations of the north Channel in the changjiang (Yangtze) estuary, China, 1880–2013: Causes and effects. *Geomorphology* 303, 30–40. doi:10.1016/j.geomorph.2017.11.014

Murray, A. S., and Wintle, A. G. (2003). The single aliquot regenerative dose protocol: Potential for improvements in reliability. *Radiat. Meas.* 37, 377–381. doi:10.1016/s1350-4487(03)00053-2

Nian, X. M., and Zhang, W. G. (2018). Application of optically stimulated luminescence dating to Late Quaternary coastal deposits in China. *Quat. Sci.* 38, 573–586. doi:10.11928/j.issn.1001-7410.2018.03.03

Nian, X. M., Zhang, W. G., Wang, Z. H., Sun, Q. L., Chen, J., and Chen, Z. Y. (2018b). Optical dating of Holocene sediments from the Yangtze River (changjiang) delta, China. *Quat. Int.* 467, 251–263. doi:10.1016/j.quaint.2018.01.011

Nian, X. M., Zhang, W. G., Wang, Z. H., Sun, Q. L., Chen, J., Chen, Z. Y., et al. (2018a). The chronology of a sediment core from incised valley of the Yangtze River delta: Comparative OSL and AMS ^{14}C dating. *Mar. Geol.* 395, 320–330. doi:10.1016/j.margeo.2017.11.008

Nian, X. M., Zhang, W. G., Wang, Z. H., Sun, Q. L., and Chen, Z. Y. (2021). Inter-comparison of optically stimulated luminescence (OSL) ages between different fractions of Holocene deposits from the Yangtze delta and its environmental implications. *Mar. Geol.* 432, 106401. doi:10.1016/j.margeo.2020.106401

Nian, X., Zhang, W., Qiu, F., Qin, J., Wang, Z., Sun, Q., et al. (2019). Luminescence characteristics of quartz from Holocene delta deposits of the Yangtze River and their provenance implications. *Quat. Geochronol.* 49, 131–137. doi:10.1016/j.quageo.2018.04.010

Niu, W. L., Zhao, L., Switzer, A. D., Zhai, Y., Zhang, W. T., and Wang, Z. H. (2021). Sedimentary evidence for a period of rapid environmental change in the Yangtze River Delta, China around 150 years ago. *Cont. Shelf Res.* 229, 104552. doi:10.1016/j.csr.2021.104552

Rees-Jones, J. (1995). Optical dating of young sediments using fine-grain quartz. *Anci. TL* 13, 9–14.

Richardson, C. (2001). Residual luminescence signals in modern coastal sediments. *Quat. Sci. Rev.* 20, 887–892. doi:10.1016/s0277-3791(00)00052-4

Sanderson, D. C. W., Bishop, P., Stark, M., Alexander, S., and Penny, D. (2007). Luminescence dating of canal sediments from angkor borei, Mekong delta, southern Cambodia. *Quat. Geochronol.* 2, 322–329. doi:10.1016/j.quageo.2006.05.032

Shen, H. T., He, S. L., Pan, D. A., and Li, J. F. (1992). A study of turbidity maximum zone in the Changjiang Estuary. *Acta Geogr. Sin.* 47, 472–479. (In Chinese with English abstract).

Shen, H. T., and Li, J. F. (2011). *Water and sediment transport in the changjiang estuary*. Beijing: China Ocean Press. (In Chinese).

Shen, H. T., and Pan, D. A. (2001). *Turbidity maximum in the changjiang estuary*. Beijing: China Ocean Press. (In Chinese).

Su, J. F., and Fan, D. D. (2018). Internal facies architecture and evolution history of changxing mouth-bar complex in the changjiang (Yangtze) delta, China. *J. Ocean. Univ. China* 17, 1281–1289. doi:10.1007/s11802-018-3814-y

Sugisaki, S., Buylaert, J. P., Murray, A., Tada, R., Zheng, H., Ke, W., et al. (2015). OSL dating of fine-grained quartz from Holocene Yangtze delta sediments. *Quat. Geochronol.* 30, 226–232. doi:10.1016/j.quageo.2015.02.021

Wang, F., Nian, X. M., Wang, J. L., Zhang, W. G., Peng, G. Y., Ge, C., et al. (2018). Multiple dating approaches applied to the recent sediments in the Yangtze River (Changjiang) subaqueous delta. *Holocene* 28, 858–866. doi:10.1177/0959683617752847

Wang, F., Zhang, W. G., Nian, X. M., Ge, C., Zhao, X. Q., Cheng, Q. Z., et al. (2019). Refining the late-Holocene coastline and delta development of the northern Yangtze River delta: Combining historical archives and OSL dating. *Holocene* 29 (9), 1439–1449. doi:10.1177/0959683619854522

Wang, J., Dai, Z. J., Mei, X. F., and Fagherazzi, S. (2020). Tropical cyclones significantly alleviate mega-deltaic erosion induced by high riverine flow. *Geophys. Res. Lett.* 47 (19), e2020GL089065. doi:10.1029/2020gl089065

Wang, J. L., Huang, D. K., Xie, W. M., He, Q., and Du, J. Z. (2021). Particle dynamics in a managed navigation channel under different tidal conditions as determined using multiple radionuclide tracers. *J. Geophys. Res. Oceans* 126 (3), e2020JC016683. doi:10.1029/2020jc016683

Wang, Y., Long, H., Yi, L., Yang, L. H., Ye, X. R., and Shen, J. (2015). OSL chronology of a sedimentary sequence from the inner-shelf of the East China Sea and its implication on post-glacial deposition history. *Quat. Geochronol.* 30, 282–287. doi:10.1016/j.quageo.2015.06.005

Warner, J. C., Butman, B., and Dalyander, P. S. (2008). Storm-driven sediment transport in Massachusetts Bay. *Cont. Shelf Res.* 28 (2), 257–282. doi:10.1016/j.csr.2007.08.008

Xu, S. Y., Shao, X. S., Chen, Z. Y., and Yan, Q. S. (1989). Studies of storm deposits in the Yangtze delta. Sci. *China (Series B)* 7, 767–773. (In Chinese).

Zhu, H. F., Yun, C. X., Mao, Z. C., and Wang, S. M. (1988). "Characteristics and empiric relationships of wind generated waves in the Changjiang estuary," in *Process of dynamics and geomorphology of the changjiang estuary: Shanghai, China*. Editors J. Y. Chen, H. T. Shen, and C. X. Yu (Shanghai: Shanghai Scientific and Technical Publishers), 166–177. (In Chinese).